BRIDGE DECK FLUTTER DERIVATIVES: EFFICIENT NUMERICAL EVALUATION EXPLOITING THEIR INTERDEPENDENCE.

F. Nieto[a], J.S. Owen[b], D.M. Hargreaves[b] & S. Hernández[a]

[a] *School of Civil Engineering, University of A Coruña, Spain*
[b] *Faculty of Engineering, University of Nottingham, UK*

ABSTRACT

Increasing the efficiency in the process to numerically compute the flutter derivatives of bridge deck sections is desirable to advance the application of CFD based aerodynamic design in industrial projects. In this paper, a 2D unsteady Reynolds-averaged Navier-Stokes (URANS) approach adopting Menter's SST k-ω turbulence model is employed for computing the flutter derivatives and the static aerodynamic characteristics of two well known examples: a rectangular cylinder showing a completely reattached flow and the generic G1 section representative of streamlined deck sections. The analytical relationships between flutter derivatives reported in the literature are applied with the purpose of halving the number of required numerical simulations for computing the flutter derivatives. The solver of choice has been the open source code OpenFOAM. It has been found that the proposed methodology offers results which agree well with the experimental data and the accuracy of the estimated flutter derivatives is similar to the results reported in the literature where the complete set of numerical simulations has been performed for both heave and pitch degrees of freedom.

KEYWORDS: Computational fluid dynamics, bluff body aerodynamics, flutter derivatives, rectangular cylinder, streamlined deck sections.

1. INTRODUCTION

Long span bridges are prone to aeroelastic phenomena such as vortex induced vibrations, flutter or buffeting. In fact, safety against flutter instability is one of the fundamental requirements in long span bridge design. If the wind speed exceeds the critical flutter speed of the structure, self-excited oscillations of the deck would rapidly amplify causing the collapse of the bridge.

The most widely used method for the identification of the flutter critical wind speed is Scanlan's approach, developed in the 1970s (Scanlan and Tomko, 1971), where a set of semi-empirical functions, named flutter derivatives, must be identified in order to define the motion-induced aerodynamic load acting on the bridge deck (Bartoli and Mannini, 2008). Traditionally, the identification of flutter derivatives has been conducted by means of wind tunnel tests of sectional models of bridge decks. The application in recent years of numerical methods in the identification of flutter derivatives aims at avoiding expensive and cumbersome experimental campaigns which are the standard approach in industrial applications currently.

In Computational Fluid Dynamics (CFD) modeling the flutter derivatives identification can be done following two different approaches (Fransos and Bruno, 2006). The first one requires the simulation of the forced harmonic oscillations in pitch and heave degrees of freedom. Then, the flutter derivatives are identified from the amplitude and phase relationships between the imposed displacement and the induced aeroelastic forces. The second method, based on indicial theory,

requires simulating an abrupt displacement of the body immersed in the flow, which causes non-stationary forces. The flutter derivatives can then be computed from the ratio between the Fourier transforms of the step-response non-stationary forces and the prescribed step-input displacement. The methodology, based on the simulation of forced oscillations, has been, by far, more widely used than the one based on the indicial approach despite the apparent efficiency of the indicial function approach.

Focusing on applications of the harmonic forced oscillations approach, the trend in the 1990's and early 2000's has been developing in-house CFD solvers based on the finite-difference, finite element, finite volume or discrete vortex methods. The references in the literature are numerous and some examples, without intending to be exhaustive are: Mendes and Branco (1998), Larsen and Walther (1998), Morgenthal and McRobie (2002), Xiang and Ge (2002), Vairo (2003), Jeong and Kown (2003), Frandsen (2004), Zhu et al. (2007) and Zhu et al. (2009). Developing in-house software has obviously been a barrier for the application of numerical methods in industrial bridge design problems due to its scientific complexity and the required labor and financial resources. Therefore more recently the focus has been put on applying general purpose commercial finite volume solvers in bridge aerodynamics problems. An early application was authored by Bruno et al. (2001) who used FLUENT for studying the aerodynamic response of a static box deck and the effect of section details such as fairings and barriers. Fluid-structure interaction problems have been addressed more recently. In Ge and Xiang (2008) both in-house solvers and the commercial code FLUENT are applied, depending on the chosen approach for turbulence modeling. Sarwar et al. (2008) obtained the flutter derivatives of a bridge deck section and high aspect ratio rectangular cylinders by means of 3D Large Eddy Simulation (LES) using FLUENT. Huang et al. (2009) also used FLUENT to compute the flutter derivatives of the Great Belt Bridge and the Sutong Yangtze cable-stayed bridge. Starossek et al. (2009) employed the commercial software COMET to obtain the flutter derivatives of 31 different bridge sections, including experimental validation for a subset of 9 sections tested in a water tunnel. Bai et al. (2010) used a combination of in-house code and ANSYS-CFX commercial software for computing force coefficients and flutter derivatives of various 3D deck sections. Huang and Liao (2011) used FLUENT to simulate forced oscillations of a flat plate and a bridge deck containing a linear combination of a set of frequencies. Also, Brusiani et al. (2013) employed FLUENT to compute the flutter derivatives of the Great Belt Bridge using a different turbulence model than Huang and co-workers. Of particular interest is the growing use of open source general CFD solvers. In Sarkic et al. (2012), the open source code OpenFOAM is applied to numerically replicate the wind tunnel test for identifying the force coefficients and flutter derivatives of a box deck cross-section. A more recent application by some of the authors of the former reference can be found in Sarkic and Höffer (2013) where the LES turbulence model is applied to the same box deck.

CFD applications based on indicial functions are scarce in spite of its potential. In Bruno and Fransos (2008) it has been remarked that in this method just a single simulation for each degree of freedom is required to identify the complete set of flutter derivatives and that only the transient flow needs to be simulated. Thus, this approach is less demanding in computational resources than the classical forced oscillation based method. On the other hand, the problem is particularly challenging from the CFD simulation perspective. Early applications are Lesieutre et al. (1994) who simulated the motion of a wing in the frame of an application to aircraft manoeuvers and Brar et al. (1996) who applied the Finite Element Method to obtain the flutter derivatives of an airfoil and a rectangular cylinder. A modified smoothed indicial approach was further developed in Fransos and Bruno (2006) and Bruno and Fransos (2008) who used FLUENT to obtain the flutter

derivatives of a flat plate of finite thickness and studied also the effect of the Reynolds number on the flutter derivatives. The indicial approach has also been applied in the frame of a probabilistic study of the aerodynamic and aeroelastic responses of a flat plate (Bruno et al, 2009). More recently Zhu and Gu (2014) have presented a method to extract the flutter derivatives of streamlined bridge decks, even if the application of the modified indicial approach to bluff bodies remains questionable.

From the previous review of the state of the art regarding applications of CFD in the design of long span bridges, the main reasons why numerical simulations are not being generally applied in bridge design in the industry to complement wind tunnel tests need to be discussed. Developing and upgrading in-house software is a complex task and requires highly skilled personnel and substantial funding. Consequently it can only be achieved by a small number of organizations in the world. The increasing use of commercial software in recent years is making it easier to access the required technology. However, the cost of licenses, particularly for running massively parallel simulations, in many cases prevents the extensive use of CFD in design problems. This circumstance has made particularly appealing the use of open source solvers for both industry and academia, and open source software has already been applied in bridge design problems. Besides this, the increasing number of published successful simulations in bridge related problems means that CFD techniques are nowadays more mature and therefore more robust and reliable.

In spite of the dramatic improvements in computational power and access to cluster technology of recent years, the computer power demands linked with modeling complex fluid-structure interaction problems remains a key issue. In this respect, any method or technique which allows decreasing computational demands would facilitate incorporating CFD based design in bridge engineering design. A number of researchers have proposed explicit relationships between flutter derivatives which have proved to be reliable for streamlined bridge decks such as Matsumoto (1996), Scanlan et al. (1997), Chen and Kareem (2002) or Tubino (2005). The application of these formulae allows the number of computer simulations for obtaining the flutter derivatives to be reduced to just half of the number required following the standard approach based on forced harmonic vibrations in heave and pitch degrees of freedom. To the authors' knowledge the aforementioned approach has not been applied in CFD-based studies to date.

The aim of the current piece of research is to propose a cost effective, and therefore efficient, computer based approach for obtaining force coefficients and flutter derivatives of bridge deck box sections which could be used in industrial applications where the shape of different bridge deck designs could be numerically optimized. Consequently, a 2D URANS strategy is proposed, using the general purpose open source CFD solver OpenFOAM v2.1.1 in combination with the explicit relationships between flutter derivatives mentioned above. The more demanding 3D Detached Eddy Simulation (DES) or LES approaches, in spite of their superior accuracy, have not been considered in this work since they would pose additional challenges in terms of higher computer power demands and model setup.

A rectangular cylinder showing a separated and reattached time-averaged flow pattern has been selected as one of the case studies for the computation of the flutter derivatives. In particular, a ratio B/H=4.9 rectangular cylinder (B is the prism width and H is the height) was chosen in order to replicate an existing sectional model at the wind tunnel of the University of Nottingham. In the literature, the number of published references, both experimental and computational, dealing with the response of B/H=5 rectangular cylinders is plentiful, to a great extent thanks to the BARC initiative (Bruno et al. 2014). Taking into account the expected minimal differences between the

aerodynamic response of *B/H*=4.9 and *B/H*=5 rectangular cylinders, for the sake of the efficiency of means in research, the authors have considered that the existing literature on 5:1 rectangular cylinders is adequate for the validation of the force coefficients and the flutter derivatives of the B/H=4.9 rectangular cylinder at 0º angle of attack. However, in the case that additional numerical studies would require validation against experimental data outside the range found in the literature, further wind tunnel tests could readily be conducted using the existing *B/H*=4.9 sectional model.

The second application case has been the G1 generic box section described in Scanlan and Tomko (1971) and Larsen and Walther (1998). The modern practice in long span bridge design has incorporated box deck cross-sections as the most common choice for these challenging structures. There are several reasons for this: a good aerodynamic and aeroelastic response characteristic of streamlined cross-sections, high torsional stiffness, construction economy and, in many cases, superior aesthetic value compared to truss girders. Recent examples of applications comprising box decks are the Forth Replacement Crossing in the United Kingdom, the Normandy Bridge and Millau Viaduct, in France, the Sutong Bridge in China or the Russky Bridge in Russia, amongst many others.

In the first part of this paper, the fundamental formulation and the numerical approach adopted, along with the computational models, for simulating the aerodynamic response of the bridge decks are explained. Then, the results of the study of the sensitivity of the solution to the spatial and temporal discretisations for the G1 generic section are summarized. Next the aerodynamic characteristics of the static *B/H*=4.9 rectangular cylinder are analyzed based on the values of the Strouhal number, force coefficients and the distribution of the averaged pressure coefficient and its standard deviation. Then the flutter derivatives of the rectangular cylinder, where the relationships between flutter derivatives have been applied, are reported and compared with wind tunnel data. It follows the analysis of the characteristics of the static G1 section based on force coefficients and the distribution of the averaged pressure coefficient. The results section ends with the report of the flutter derivatives of the G1 section and the corresponding comparison with experimental and other numerical data in the literature. Finally, conclusions are drawn from the work reported herein.

2. NUMERICAL FORMULATION

The flow around the bluff bodies of interest is modeled by means of the unsteady Reynolds-averaged Navier-Stokes equations considering incompressible flow. A 2D URANS approach has been preferred which, according to Brusiani et al. (2013), is equivalent to imposing the perfect correlation of the flow structures in the span-wise direction.

The time averaging of the equations for conservation of mass and momentum gives the Reynolds averaged equations of motion in conservative form. According to Wilcox (2006):

$$\frac{\partial U_i}{\partial x_i} = 0 \tag{1.a}$$

$$\rho \frac{\partial U_i}{\partial t} + \rho U_j \frac{\partial U_i}{\partial x_j} = -\frac{\partial P}{\partial x_i} + \frac{\partial}{\partial x_j}\left(2\mu S_{ij} - \rho\overline{u_i' u_j'}\right) \tag{1.b}$$

where U_i is the mean velocity vector, x_i is the position vector, t is the time, ρ is the fluid density, assumed constant, u_i' is the fluctuating velocity and the overbar represents the time average, P is

the mean pressure, μ is the fluid viscosity and S_{ij} is the mean strain-rate tensor. From the above equation, the specific Reynolds stress tensor is defined as:

$$\tau_{ij} = -\overline{u_i' u_j'} \tag{2}$$

which is an additional unknown to be modeled based on the Boussinesq assumption for one and two equation turbulence models (Wilcox, 2006).

$$\tau_{ij} = 2\nu_T S_{ij} - \frac{2}{3} k \delta_{ij} \tag{3}$$

where ν_T is the kinematic eddy viscosity, S_{ij} is the mean strain-rate tensor and k is the turbulent kinetic energy per unit mass.

In this work the closure problem is solved applying Menter's *k-ω* SST model for incompressible flows, reported in Menter and Esch (2001).

For the simulations where forced oscillations of the bluff body have been imposed, the Arbitrary Lagrangian Eulerian (ALE) formulation has been applied for allowing movements of the mesh inside the computational domain. The conservation of mass and momentum equations are written as follows (Bai et al., 2010, Sarkic et al., 2012):

$$\frac{\partial (U_i - U_{gi})}{\partial x_i} = 0 \tag{4.a}$$

$$\rho \frac{\partial U_i}{\partial t} + \rho U_j \frac{\partial (U_i - U_{gi})}{\partial x_j} = -\frac{\partial P}{\partial x_i} + \frac{\partial}{\partial x_j}\left(2\mu S_{ij} - \rho \overline{u_i' u_j'}\right) \tag{4.b}$$

where U_{gi} is the grid velocity in the *i*-th direction.

3. FORCE COEFFICIENTS AND FLUTTER DERIVATIVES COMPUTATION BY MEANS OF FORCED OSCILLATION SIMULATIONS

The definition of the force coefficients considered in this study is given in (5):

$$C_d = \frac{D}{\frac{1}{2}\rho U^2 B} \qquad C_l = \frac{L}{\frac{1}{2}\rho U^2 B} \qquad C_m = \frac{M}{\frac{1}{2}\rho U^2 B^2} \tag{5}$$

In the former expressions D is the drag force per span length, positive in the windward direction, L is the lift force per span length, positive upwards, and M is the pitching moment per span length, positive clockwise, ρ is the fluid density, U is the flow speed and B is the bluff body width.

Flutter derivatives are semi-empirical parameters which relate motion-induced forces ~~and~~ with the displacements of the structure and their time derivative. These parameters have traditionally been identified using wind tunnel tests, but more recently, numerical based simulations have been applied.

According to Simiu and Scanlan (1996), the aeroelastic forces on a bridge deck, considering two degrees of freedom (heave and pitch), can be written as follows:

$$L_{ae} = \frac{1}{2}\rho U^2 B\left[KH_1^*\frac{\dot{h}}{U} + KH_2^*\frac{B\dot{\alpha}}{U} + K^2H_3^*\alpha + K^2H_4^*\frac{h}{B}\right] \quad (6.a)$$

$$M_{ae} = \frac{1}{2}\rho U^2 B^2\left[KA_1^*\frac{\dot{h}}{U} + KA_2^*\frac{B\dot{\alpha}}{U} + K^2A_3^*\alpha + K^2A_4^*\frac{h}{B}\right] \quad (6.b)$$

where L_{ae} is the aeroelastic force per unit of span length, M_{ae} is the aeroelastic moment per unit of span length, ρ is the fluid density, U is the flow speed, $K = (B\omega)/U$ is the reduced frequency, B is the deck width, ω the circular frequency of oscillation, h is the heave displacement, α is the torsional rotation, $\dot{h}$ and $\dot{\alpha}$ are the time derivatives and H_i^* and A_i^* $(i = 1, \dots, 4)$ are the flutter derivatives.

Assuming prescribed harmonic forced oscillations $h = h_0 e^{i\omega t}$ and $\alpha = \alpha_0 e^{i\omega t}$, where h_0 and α_0 are the amplitudes of the oscillations, and also that motion-induced forces are linear functions of the movement; after some manipulation, the following expressions are obtained for the identification of the flutter derivatives:

$$H_1^* = -\left(\frac{U}{Bf}\right)^2 \frac{C_l \sin\varphi_{L-h}}{(2\pi)^2\, h_0/B} \quad (7.a) \qquad A_1^* = -\left(\frac{U}{Bf}\right)^2 \frac{C_m \sin\varphi_{M-h}}{(2\pi)^2\, h_0/B} \quad (7.e)$$

$$H_2^* = -\left(\frac{U}{Bf}\right)^2 \frac{C_l \sin\varphi_{L-\alpha}}{(2\pi)^2\alpha_0} \quad (7.b) \qquad A_2^* = -\left(\frac{U}{Bf}\right)^2 \frac{C_m \sin\varphi_{M-\alpha}}{(2\pi)^2\alpha_0} \quad (7.f)$$

$$H_3^* = \left(\frac{U}{Bf}\right)^2 \frac{C_l \cos\varphi_{L-\alpha}}{(2\pi)^2\alpha_0} \quad (7.c) \qquad A_3^* = \left(\frac{U}{Bf}\right)^2 \frac{C_m \cos\varphi_{M-\alpha}}{(2\pi)^2\alpha_0} \quad (7.g)$$

$$H_4^* = \left(\frac{U}{Bf}\right)^2 \frac{C_l \cos\varphi_{L-h}}{(2\pi)^2\, h_0/B} \quad (7.d) \qquad A_4^* = \left(\frac{U}{Bf}\right)^2 \frac{C_m \cos\varphi_{M-h}}{(2\pi)^2\, h_0/B} \quad (7.h)$$

where φ_{L-h}, $\varphi_{L-\alpha}$, φ_{M-h} and $\varphi_{M-\alpha}$ are the phase lags of the fluctuating aeroelastic lift and moment with respect to the heave and pitch harmonic oscillations and C_l and C_m are the amplitudes of the non-dimensional aeroelastic lift and moment.

It must be borne in mind that in Larsen and Walther (1998), whose results are used later for validation, the flutter derivatives are computed dividing equations (7.a) to (7h.) by 2.

4. RELATIONSHIPS BETWEEN FLUTTER DERIVATIVES

As mentioned in the introduction, a number of publications can be found in the literature reporting several relationships amongst flutter derivatives. Tubino (2005) has derived the following relationships between heave-related and pitch-related flutter derivatives assuming the linear formulation hypothesis for the self-excited forces:

$$H_1^*(K) = KH_3^*(K) - \frac{C_d}{K} \quad (8.a) \qquad A_1^*(K) = KA_3^*(K) \quad (8.c)$$

$$H_4^*(K) = -KH_2^*(K) \quad (8.b) \qquad A_4^*(K) = -KA_2^*(K) \quad (8.d)$$

The above equations are similar to the ones reported by Matsumoto (1996) apart from the (H_1^*, H_3^*) relationship, that does not consider the term containing the drag coefficient. For streamlined sections with low drag coefficient its contribution is nearly negligible.

Experimental validation of the former relationships reported in Tubino (2005), has shown that the relationships between (H_1^*, H_3^*) and (A_1^*, A_3^*) were satisfied for all the cases considered while the relationships between (H_2^*, H_4^*) and (A_2^*, A_4^*) were closely verified for streamlined deck cross-sections, since minor discrepancies are identified between experimental realizations and the approximated values. In Matsumoto (1996), the reported relationships between flutter derivatives are confirmed for rectangular cylinders less affected by vortex generation, proposing as a reference lower bound a 5:1 ratio.

5. GEOMETRY AND COMPUTER MODELING

Two different geometries have been considered as case studies in the present work: a *B/H*=4.9 rectangular cylinder (*H* is the section ~~depth or~~ height), and the generic G1 deck section, described in Larsen and Walther (1998), representative of streamlined box decks.

5.1. B/H=4.9 rectangular cylinder

Figure 1 shows the layout of the flow domain and boundary conditions employed in the rectangular cylinder simulations. The flow domain considered for the rectangular cylinder case is 40.8*B* by 30*B* similar to the size employed in successful simulations by other researchers such as Fransos and Bruno (2010).

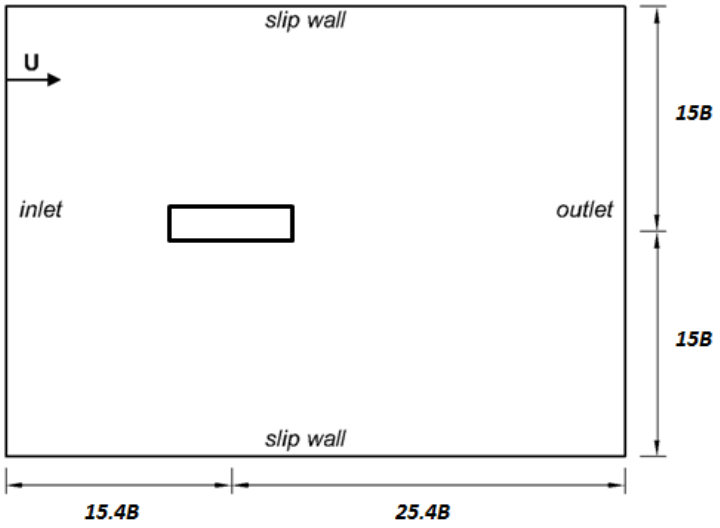

Figure 1. Flow domain definition and boundary conditions for the B/H=4.9 rectangular cylinder (not to scale).

A constant velocity inlet has been set at the upwind boundary (the left side in the figure) of the computational domain. The incoming flow has a turbulence intensity of 1 % along with a 0.1*B* turbulent length scale as per Ribeiro (2011). A pressure outlet at atmospheric pressure has been imposed at the right side (see figure 1). The upper and lower boundaries have been defined as slip walls. The corners of the prism have been modeled as sharp and its walls are defined as non-slip. When the rectangular cylinder is forced to oscillate the resultant velocity field around the

rectangular cylinder wall is corrected, so that the velocity of the flow at the moving boundary is equal to the mesh velocity and therefore no flux across the wall takes place.

The numerical schemes adopted in the simulations reported herein are summarized next. The interpolation of values from the cell centers to face centers is done using a linear scheme. The gradient terms are discretised using the Gauss scheme with a linear interpolation scheme. For the divergence terms, the Gauss scheme is also selected, adopting linear upwind and limited linear interpolation schemes. For the Laplacian terms the choice has been the Gauss scheme with a linear interpolation scheme and a limited surface normal gradient scheme. The Euler first order bounded implicit scheme was set for the first time derivative terms.

A block structured mesh with ~~a~~ topology similar to the one in Braun and Awruch (2003), has been generated. The total number of cells is 148320, and the number of cells around the walls of the rectangular cylinder is 460. For the first layer of cells, the height to width ratio is $\delta_1/B = 5.11 \times 10^{-4}$, for which the mean value of the non-dimensional height ($y^+ = (\delta_1 u_*)/\nu$, where δ_1 is the height of the first prismatic grid layer around the deck and u_* is the friction velocity) is about 1.8 and the maximum value is close to 8 at $Re = 1.01 \times 10^5$. These bounds are ~~the~~ similar to those reported in Sarkic et al. (2012), and in this model, the number of cells with $y^+ > 4$ is about 5% of the total number of cells around the rectangular cylinder and they are located mainly in the windward corners. In both static and forced harmonic oscillations a maximum Courant number of 1 has been imposed, which produces for the static prism at the Reynolds number of reference a mean non-dimensional time step $\overline{\Delta s} = \overline{\Delta t} U/B = 6.7 \times 10^{-4}$. The abundant literature reporting numerical studies on rectangular cylinders means verification studies concerning mesh size and time step refinements for the rectangular cylinder case can be avoided, since the authors have used common mesh topologies and have adopted mesh characteristics and a time step more demanding than other successful simulations.

5.2. G1 generic deck cross-section

The detailed geometry of the G1 generic cross-section is depicted in figure 8. The flow domain size in this case is 37B by 27B (B is the deck width), similar to the size employed in the rectangular cylinder case. The boundary conditions are the same as in the rectangular cylinder case.

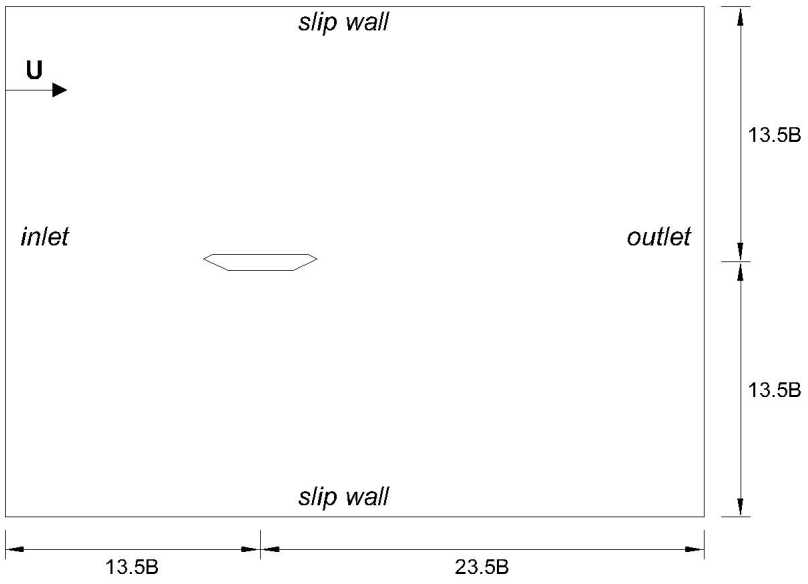

Figure 2. Flow domain definition and boundary conditions for the G1 section (not to scale).

To verify the spatial discretisation, for the streamlined G1 deck section three different grids, with different mesh densities, have been considered for the static deck case with a 0º angle of attack. The meshes are identified as Coarse, Medium and Fine grids. In all the cases, a 2D block structured regular mesh has been used. A high density mesh has been defined around the deck cross-section, the so-called boundary layer mesh, taking special care in order to obtain maximum values for the first grid non-dimensional height y^+ below 4, which is a more demanding bound than the one set by Sarkic et al. (2012) for a similar problem. In this manner, no wall functions are required and the turbulence model equations are integrated along the viscous sublayer. The thickness of this layer is *B*/25. The Coarse mesh comprises 25 rows of elements in this zone and the height of the first element around the cross-section is defined as $\delta_1/B = 2.08 \times 10^{-4}$, while the expansion ratio between the end cell and the start cell is 25. For the Medium (Figure 3) and Fine meshes the boundary layer definition was identical: 50 rows considering an expansion ratio of 10, which gives a first cell non-dimensional height $\delta_1/B = 2.03 \times 10^{-4}$, very close to the Coarse mesh case in order to be able to drive conclusions from the verification analyses since the y^+ values are comparable for the three cases. For a Reynolds number $Re = 1.07 \times 10^5$, these mesh arrangements offer a mean value of the y^+ around the deck close to 1, with a very limited number of cells with $y^+ > 2$ located at the windward corners of the deck. The maximum value of y^+ for the three cases is about 3.7.

In table 1 the total number of cells, the number of cells around the deck section and the integral aerodynamic parameters are reported along with the standard deviation (prime symbol) values of the force coefficients for each mesh.

Table 1. Properties and results of the grid-refinement study for the G1 section.

Grid	Total cells	Cells around deck	S_t	C_d	C_l	C_m	C'_d	C'_l	C'_m
Coarse	149600	640	0.20	0.056	-0.026	0.035	0.0003	0.010	0.0022
Medium	268150	770	0.19	0.057	-0.033	0.034	0.0006	0.022	0.0047
Fine	363300	770	0.19	0.057	-0.034	0.034	0.0006	0.022	0.0047

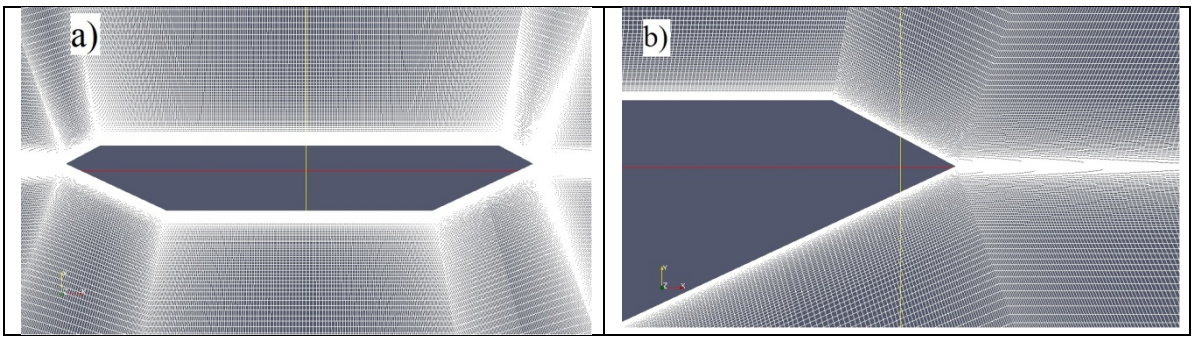

Figure 3. G1 section block structured grid: a) close-up of the deck and b) detail around the lee-ward corner of the deck.

The main discrepancies found have been the lower values in the standard deviation of the force coefficients and the slight underestimation of the lift coefficient when the coarse mesh has been

used. Consequently the Coarse mesh has been disregarded and Medium mesh is adopted hereafter since the results are similar to the ones obtained using the Fine mesh at a lower computational cost.

Regarding the analysis of the sensitivity of the solution depending on the chosen time step, two different maximum Courant numbers equal to 1 and 0.5 have been considered in order to check the influence of the temporal discretisation (Mannini et al., 2010). In table 2, where the non-dimensional time step is defined as $\overline{\Delta s} = \overline{\Delta t} U/B$, the numerical results obtained are reported, finding that they offer very close figures; therefore the higher maximum Courant number is retained for the remaining simulations.

Table 2. Results of the time-refinement study for the G1 section.

Max. Co. numb.	$\overline{\Delta s}$	S_t	C_d	C_l	C_m	C'_d	C'_l	C'_m
1	3.5e-4	0.19	0.057	-0.033	0.034	0.0006	0.022	0.0047
0.5	1.8e-4	0.20	0.058	-0.037	0.034	0.0006	0.019	0.0040

5.3. Grid movement strategy

The computer implementation of the ALE formulation requires a mesh-update method that assigns mesh-node velocities or displacements at each calculation time step (Donea et al., 2004).

In the simulations conducted in this research the boundary motion is defined by the prescribed forced oscillations of the bluff body, which follows a sinusoidal law with given frequency and amplitude. On the other hand, the exterior boundaries of the fluid domain are fixed along the simulations. The whole mesh is allowed to deform between the moving and fixed boundaries.

Amongst the available mesh movement algorithms a Laplacian smoothing technique for each component of the node-mesh position has been chosen (Oliver, 2009). According to Jasak and Rusche (2009), the Laplace equation can be expressed as:

$$\nabla \cdot k \nabla \mathbf{u} = 0 \tag{9}$$

where **u** is the node-mesh displacement vector and *k* is the diffusion coefficient.

In this work the mesh control is achieved by computing the motion of the grid points solving the Laplace equation with variable diffusivity using a method based on the quadratic inverse distance from the oscillating boundary. This prevents the distortion of the smallest elements around the rectangular cylinder (Löhner, 2008).

5.4. Forced oscillations characteristics and application of relationships between flutter derivatives

With the aim of limiting the computational cost of obtaining the set of 8 flutter derivatives, the relationships between flutter derivatives (8.a–8.d) reported in Tubino (2005) are applied. As a consequence, only half of the simulations are required, which represents a substantial reduction in the computational demands of the problem. The pitch degree of freedom has been chosen as the one for carrying out the numerical simulations; therefore the H_2^*, H_3^*, A_2^* and A_3^* flutter derivatives are computed by means of the CFD simulations, while the H_1^*, H_4^*, A_1^* and A_4^* flutter derivatives are estimated using equations (8.a) to (8.d). The amplitude of the forced oscillations in the present work is $\alpha_0 = 1°$ for the two considered application examples. The sign convention adopted herein

has been the same as in Sarkar et al. (2009): heave and aeroelastic lift force positive downward, while the aeroelastic moment and rotation have been considered positive for a nose-up rotation.

6. RESULTS AND DISCUSION

6.1 B/H=4.9 rectangular cylinder

6.1.1 Flow simulation around the static *B/H*=4.9 rectangular cylinder

In table 3 the Strouhal number, the mean drag coefficient and the standard deviation of the lift and drag coefficients at $Re = 1.01 \times 10^5$ are presented along with experimental data from Schewe (2009) and the numerical data computed using two different 2D URANS approaches. The URANS references which have been considered for comparison are: Ribeiro (2011) who reports, amongst others, the results of a Reynolds Stress Model (RSM) simulation and Mannini et al. (2011) where the Linearised Explicit Algebraic (LEA) version of the Explicit Algebraic Reynolds Stress Model (EARSM) coupled with the standard *k-ω* turbulence model is employed. It must be borne in mind that in the references used for validation the ratio of the rectangular cylinder is *B/H*=5. In table 3, the reference dimension for drag coefficient and the standard deviations is *B*, therefore the data in Mannini et al. (2011), Ribeiro (2011) and Schewe (2009) which are based on *H*, have been modified for comparison. For the simulation of the *B/H*=4.9 static rectangular cylinder the simulated length has been about 100 non-dimensional time units and the reported results in table 3 have been averaged along a non-dimensional time $s = tU/B = 74$.

Table 3. *B/H*=4.9 rectangular cylinder: Strouhal number and force coefficients.

	S_t	C_d	C'_d	C'_l
Present simulation	0.123	0.227	0.0049	0.193
Mannini et al. (2011) – LEA *k-ω*	0.094	0.212	0.0038	0.215
Ribeiro (2011) - RSM	0.073	0.234		0.18
Schewe, (2009) – EXP.	0.111	0.206		≈0.08

Table 3 shows a good agreement with the experimental and numerical data, particularly taking into account that, since the aspect ratio of the rectangular cylinder considered in the simulation is lower than 5, it must show slightly higher values for both Strouhal number and drag force coefficients according with the trend in drag coefficient and Strouhal number for rectangular cylinders with aspect ratios between 4 and 6, reported in Shimada and Ishihara (2012). It is notable how Menter's *k-ω* SST turbulence model considered in this simulation offers results comparable with the sophisticated LEA approach in Mannini et al. (2011). The proximity of the Strouhal number in this simulation to the experimental value obtained in Schewe (2009) should also be highlighted and therefore a better prediction of this parameter than in Ribeiro (2011) has been obtained.

As a further validation of the reported simulations, in figure 4 the side-averaged (between the upper and lower half perimeters) and time-averaged distribution of the pressure coefficient C_p of the static ratio *B/H*=4.9 rectangular cylinder are reported along with the results in Mannini et al. (2010) for the *k-ω* LEA turbulence model, Ribeiro (2011) for the RSM and the statistics for the CFD realizations reported in Bruno et al. (2014). The side-averaged and time-averaged pressure coefficient of the ratio 4.9 rectangular cylinder is very close to the median values on the long side of the rectangular cylinder (*l/H* between 0.7 and 5.3, being *l* the length along the half of the perimeter of the rectangular cylinder, as it is described in figure 4) which indicates that the accuracy of the simulation is comparable with the CFD realizations in the frame of the BARC

initiative. Furthermore, the numerical results correctly reproduce the experimental data for the 5:1 rectangular cylinder, bearing in mind the scatter in the wind tunnel tests available in the literature.

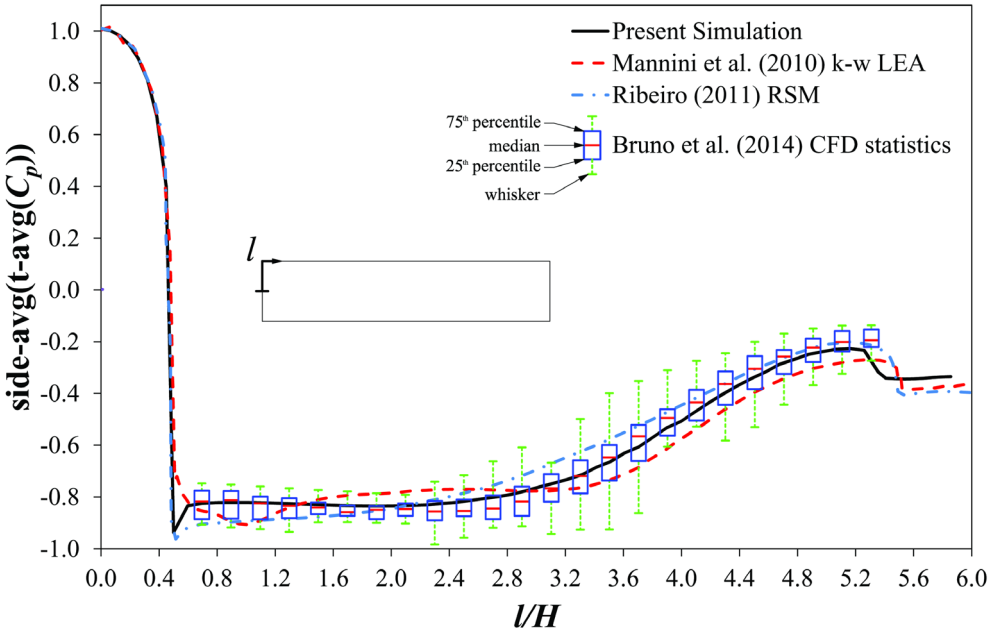

Figure 4. Side-averaged and time-averaged C_p distributions around *B/H*=4.9 and *B/H*=5 rectangular cylinders.

In figure 5, the side-averaged distribution of the standard deviation ~~in time~~ of the pressure coefficient is reported along with the statistical data for the CFD realizations in Bruno et al. (2014) and the simulations in Mannini et al. (2010) and Ribeiro (2011). In Bruno et al. (2014) the scatter in the distribution of the standard deviation of the pressure coefficient has been shown for both experimental and numerical realizations. The standard deviation distribution of the C_p reported for the *B/H*=4.9 rectangular cylinder is well inside the boundaries of the BARC realizations and it is particularly close to the RSM simulation in Ribeiro (2011). It has reported in Bruno et al. (2014) that RANS simulations present a minimum in the standard deviation of the pressure coefficient at about 2*H* from the windward corner. This minimum is also present in the simulation reported in this work.

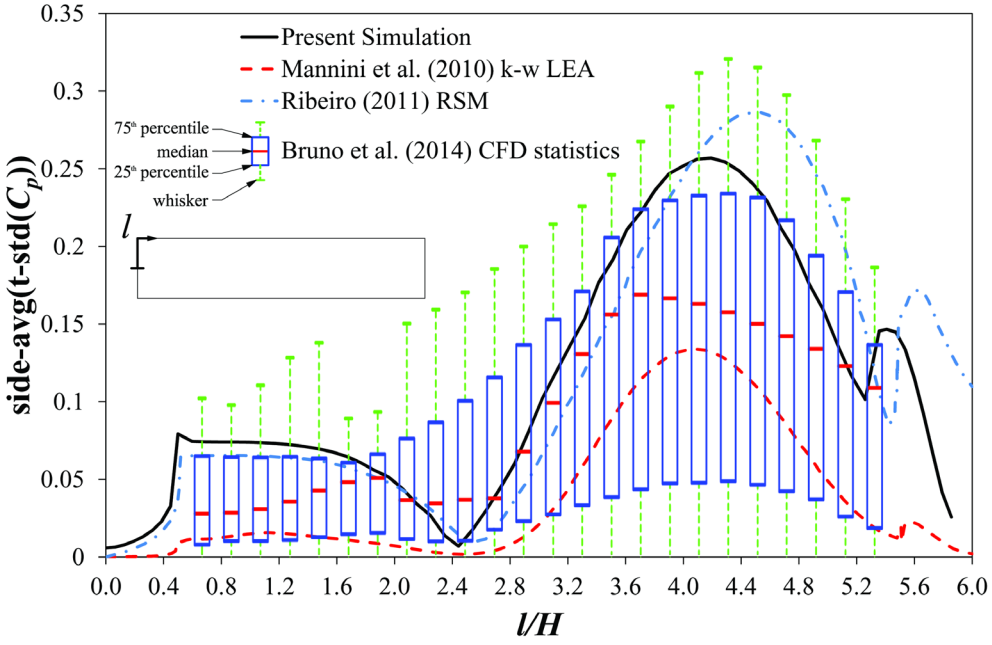

Figure 5. Side-averaged distributions around *B/H*=4.9 and *B/H*=5 rectangular cylinders of the standard deviation in time of C_p.

Based on the comparison of the drag coefficient, the standard deviation of the lift coefficient, the Strouhal number and the distribution to the time-averaged and time-standard deviation of the pressure coefficient, the agreement of the present simulation with the experimental and numerical data in the literature can be considered adequate.

6.1.2 Flutter derivatives of the *B/H*=4.9 rectangular cylinder

The flutter derivatives for the aspect ratio 4.9 rectangular cylinder have been computed over a range of reduced velocities $U_R = U/(f \cdot B)$ =(0.88, 26.40). In order to cover the whole range of reduced velocities, three frequencies of oscillation have been considered (0.5 Hz., 1 Hz. and 3 Hz.) in conjunction with flow speeds between 1 m/s and 7 m/s, which means that the range of covered Reynolds number is between 2.52×10^4 and 1.76×10^5. In some cases (U_R =2.6, 5.3, 10.6 and 15.84), the same reduced velocity has been computed with different combinations of flow velocity and frequency of oscillation in order to verify the independence of the results with the combination of both parameters.

Since the same mesh has been retained for all the simulations, the non-dimensional height y^+ reaches a maximum value close to 11 for the maximum Reynolds number ($Re = 1.76\times10^5$; $U = 7$ m/s), while the mean value of y^+ is about 2.7. For the minimum Reynolds number ($Re = 2.52\times10^4$; $U = 1$ m/s), the maximum y^+ reaches a value close to 3.5 and the mean value of y^+ is 0.6. With the aim of ascertaining the effect of the differences in the y^+ numbers on the simulations at the lower and upper bounds of the Reynolds number, as well as the dependency of the aerodynamic characteristics with the Reynolds number, the side-averaged and time-averaged along with the side-averaged time-standard deviation distributions of the pressure coefficient are presented for $U = 1$ and $U = 7$ m/s (Figure 6).

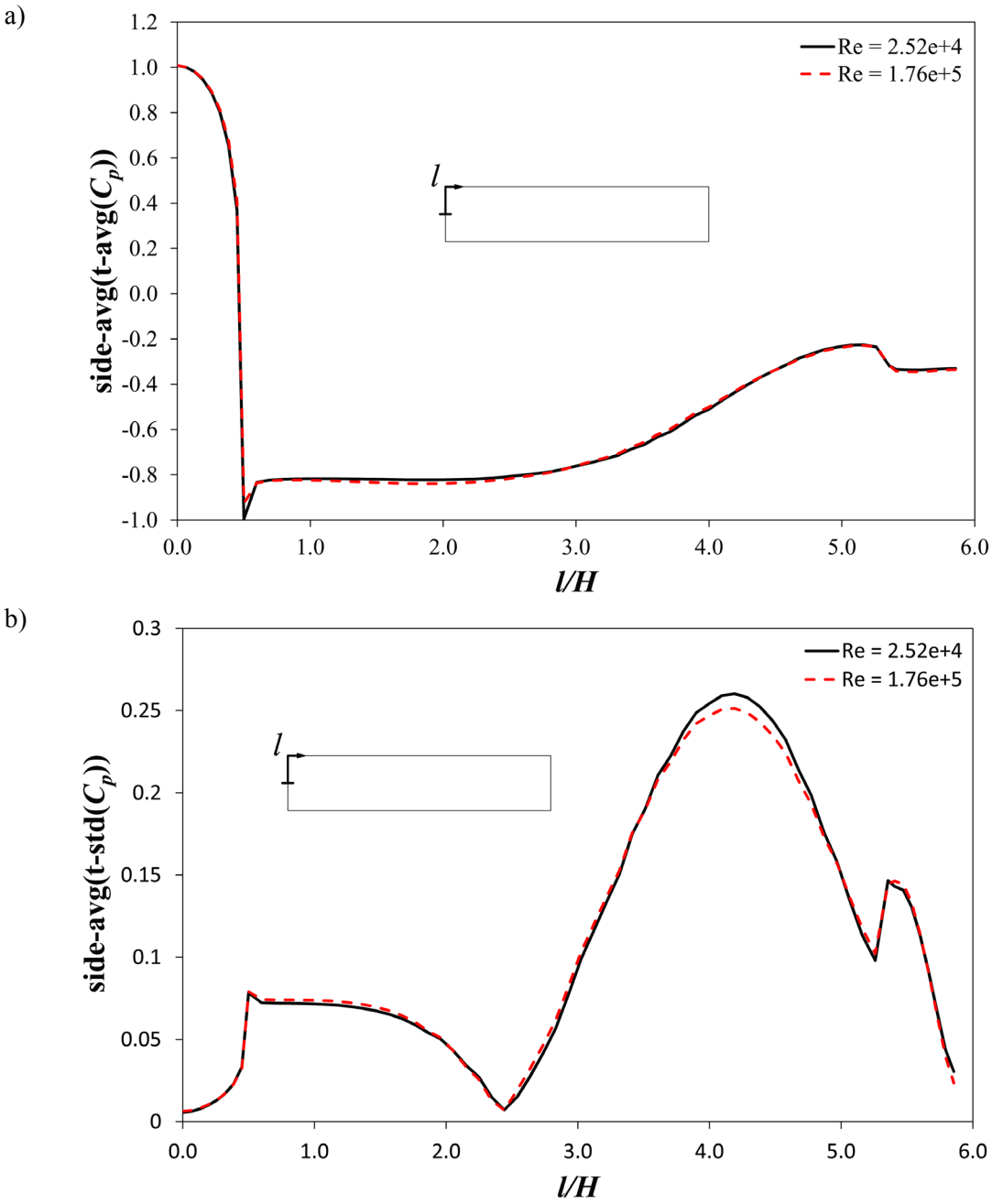

Figure 6. Side-averaged distributions around *B/H*=4.9 rectangular cylinder of the a) time-averaged and b) time-standard deviation of C_p for $U = 1$ and $U = 7$ m/s.

Figure 6 shows similar results for the side-averaged distributions of the time-averaged and the standard deviation of the pressure coefficient. Only small differences in the peak value of the distribution of the standard deviation of the pressure coefficient around the rectangular prism can be identified. Consequently, the relatively high values of the maximum y^+ at $U = 7$ m/s do not jeopardize the accuracy of the simulation. At the same time, the aerodynamic characteristics of the static sharp edged rectangular cylinder at 0º angle of attack seems to be quite insensitive to the Reynolds number, as it has been reported in Holmes (2007), citing Scruton (1981). Besides this, in the set of reduced velocities considered for the computation of the flutter derivatives, the maximum flow speed of 7 m/s is adopted for a single reduced velocity $U_R = 18.48$. In the same manner, the flow speed of 6 m/s is employed only for repeated values of $U_R = 5.3$ and $U_R = 15.84$. Therefore,

in the set of flutter derivatives which are presented next, the majority of the simulations have been conducted at $Re \leq 1.26 \times 10^5$.

In figure 7 the flutter derivatives computed from these simulations are reported along with the experimental data in Matsumoto (1996). The length of the simulations reported in the following has been between 40 and 260 non-dimensional time units, depending on the flow speed and the frequency of oscillation.

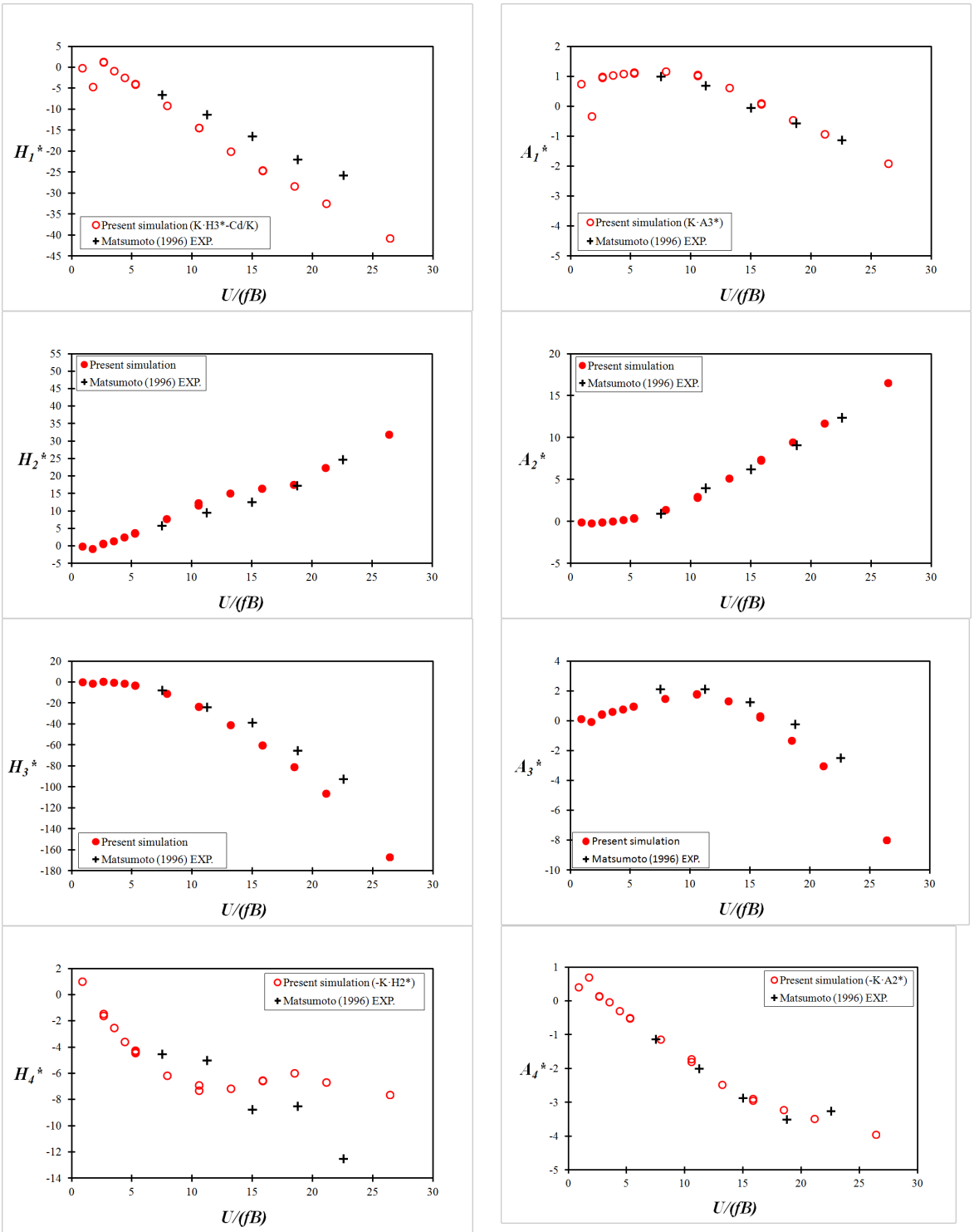

Figure 7. Flutter derivatives of the *B/H*=4.9 rectangular cylinder: computed flutter derivatives and comparison with experimental data in Matsumoto (1996).

The estimated flutter derivatives agree well with the experimental data and only the H_4^* flutter derivative shows some discrepancies with the wind tunnel values. These differences in H_4^* are comparable with the ones found in CFD simulations where forced oscillations in the heave degree of freedom have been conducted, such as in Sarwar et al. (2008) for a *B/H*=20 rectangular cylinder or Huang (2009). There are no significant differences for the repeated simulations at the same reduced velocities, which points out the relative independence of the results with the various combinations of flow speed and frequency of oscillation.

6.2 G1 generic deck cross-section

6.2.1 Flow simulation around the static G1 section

The drag coefficient, the root mean square of the lift coefficient time history and the Strouhal number of the G1 section for 0º angle of incidence computed in this study are compared in table 4 with the numerical results reported in Larsen and Walther (1998) who applied the Discrete Vortex Method in their simulations. In this case the numerical simulation of the static G1 section has been extended along 65 non-dimensional time units. The time statistics have been obtained from the final 45 non-dimensional time units.

Table 4. Static G1 section: drag coefficient, RMS of the lift coefficient and Strouhal number.

	C_d	C_l^{RMS}	S_t
Present simulation	0.06	0.04	0.19
Larsen and Walther (1998)	0.08	0.07	0.17

The agreement amongst the results for the 0º angle of attack is reasonable, however as a further validation of the numerical approach chosen by the authors, the time-averaged pressure coefficient distribution along the deck is going to be presented and compared with the experimental data reported in Sarkic et al. (2012), where the time-averaged pressure coefficient distribution along a bare box deck is provided. For further comparison, the experimental data in Bruno and Khris (2003) (taken from Larose, 1992) of the smooth flow tests of a taut strip model of the Great Belt Bridge fitted with barriers, has also been included. The geometry of the deck and the position of the pressure probes in the aforementioned reference are taken from Davenport et al. (1992). The distribution of the ~~time~~ standard deviation of the pressure coefficient is not reported since the unsteadiness of the flow was rather weak, providing values of the pressure coefficient standard deviation well below the available experimental data, particularly on the windward half of the cross section. A similar behavior is described in Sarkic et al. (2012). In figure 8, the geometry of the bridge decks considered for validation is described, while in figure 9 the time-averaged pressure coefficient distribution is shown.

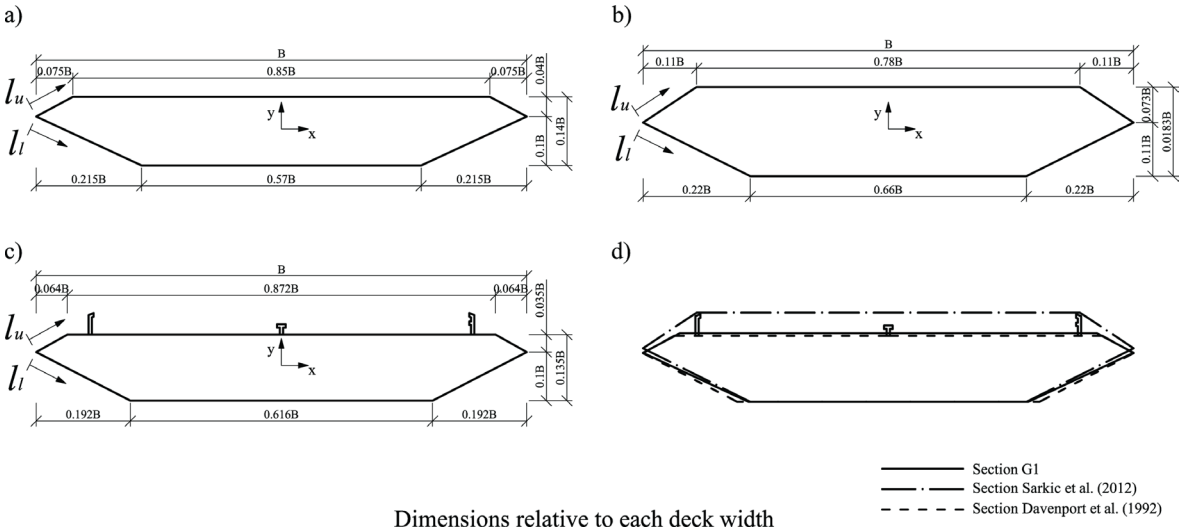

Figure 8. Geometry: a) G1 section b) section in Sarkic et al. (2012) c) section in Davenport et al. (1992) d) comparison between sections.

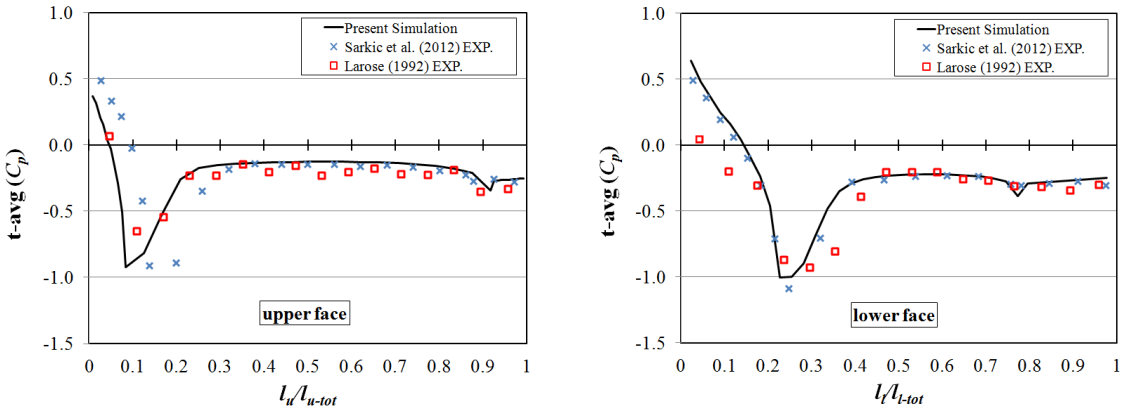

Figure 9. Time-averaged pressure coefficient distribution: numerical results and comparison with experimental data in Sarkic et al. (2012) and Larose (1992).

The agreement in the pressure coefficient distribution between the numerical simulation and the wind tunnel data in Sarkic et al. (2012) is good. On the upper face, the peak values at the windward corner are correctly simulated and the lateral shift is due to the differences in the geometry in the upper surface (see figure 8). Also the mean pressure distribution along the horizontal and the leeward plates have been accurately obtained. The agreement is even better on the lower surface, since the geometry of the two sections is nearly identical. In the authors' opinion the similitude in the Reynolds number ($Re \approx 1 \times 10^5$) of the numerical simulation and the wind tunnel test has contributed to this close agreement.

When the numerical results are compared with the wind tunnel data from Larose (1992), some discrepancies can be identified, which can arguably be related to the difference in the Reynolds number of the wind tunnel tests ($Re=7 \times 10^4$) as well as the presence of the barriers in the tested model. Besides this, discrepancy in the moderate suction on the windward surface in the lower side of the deck has already been commented in Bruno and Khris (2003).

In order to provide a more complete view of the aerodynamic characteristics of the static G1 cross section, the force coefficients in the range of angles of attack (-10º, 10º) are computed with an interval of 2º. The results are compared with the experimental data reported in Reinhold et al.

(1992) for the H4.1 section of the Great Belt Bridge design studies and the 2D numerical results published in Bai et al. (2010), for the G1 section.

Figure 10 shows the force coefficients of the G1 section. A very good agreement has been obtained between the computational results and the experimental data for the similar geometry of the H4.1 box deck section. In fact, the change in the slope of the moment coefficient for angles of incidence higher than 6º has been correctly captured as well as the step increment in the drag coefficient also for angles of attack higher than 6º. The accuracy of the slopes in the vicinity of 0º for both lift and moment coefficients should also be noted.

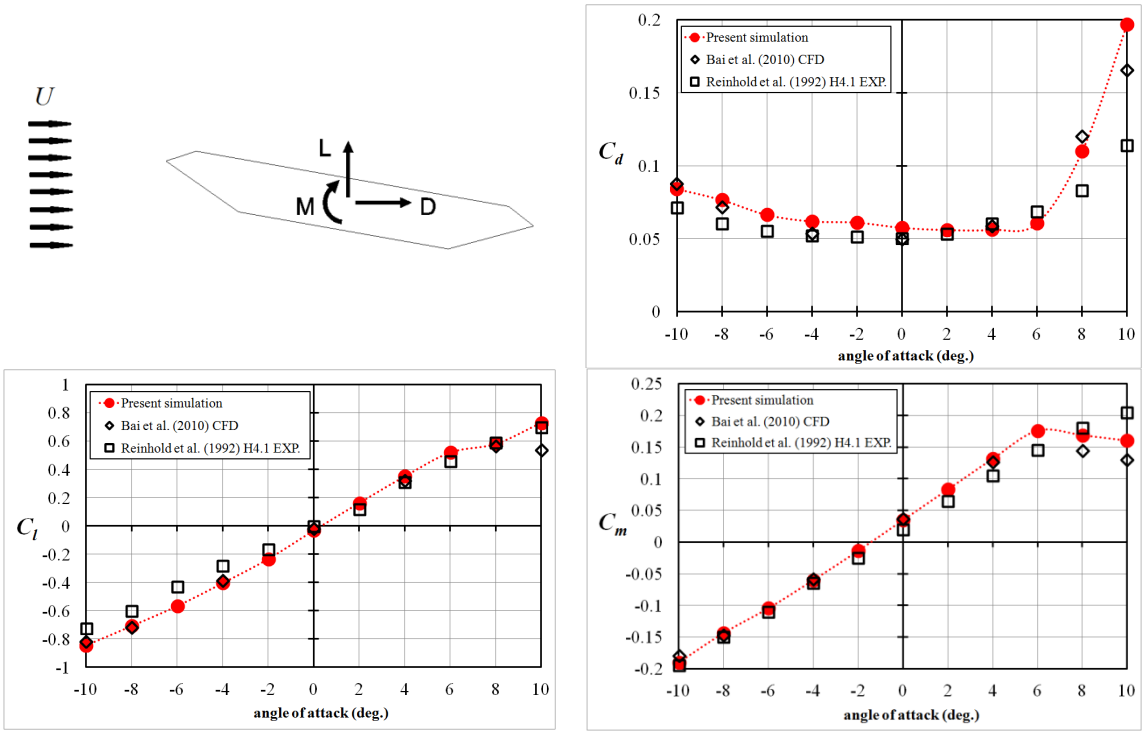

Figure 10. G1 section force coefficients: numerical results and comparison with experimental (Reinhold et al., 1992) and other numerical data (Bai et al., 2010).

6.2.2 Flutter derivatives of the G1 section

In order to identify by means of a computational approach the flutter derivatives of the G1 generic section, forced oscillation simulations were carried out at reduced velocities $U/(fB)$ equal to 2, 4, 6, 8 10 and 12, as in Larsen and Walther (1998). Also, the formulae applied for identifying the flutter derivatives are the ones reported in Larsen and Walter (1998) and Bai et al (2010), therefore the expressions in equations (7.a) to (7h) are divided by 2. The same procedure as in the rectangular cylinder case has been applied for decreasing the computational cost. As a consequence, instead of 12 computer simulations, only 6 are required, one for each reduced velocity considered. In this case the flow velocity is the same in all the simulations and the frequency of oscillation is modified in the range (0.833, 5) Hz in order to obtain the reduced velocities of interest. The solution for the fixed G1 section has been set as the initial condition for the forced oscillation simulations. Since this allows shortening the initial transient, the computations have been extended for about 50 non-dimensional time units. For the highest value of the reduced velocity, U_R=12, four complete oscillation periods have been simulated, which is greater than the 2.5 periods span adopted in Larsen and Walther (1998).

In figure 11 the numerical results obtained for H_i^* and A_i^* $(i = 1, \ldots, 3)$ are compared with the experimental ones reported in Scanlan and Tomko (1971). The numerical results obtained by Larsen and Walther (1998), and Bai et al. (2010) for the same deck section are also included in the charts. Since no experimental results are available for the H_4^* and A_4^* flutter derivatives of the G1 cross-section, the results for the H_4^* flutter derivative of the H4.1 section in Reinhold et al (1992) are provided. No experimental data for the A_4^* flutter derivative of the H4.1 section are available in the literature to the authors' knowledge.

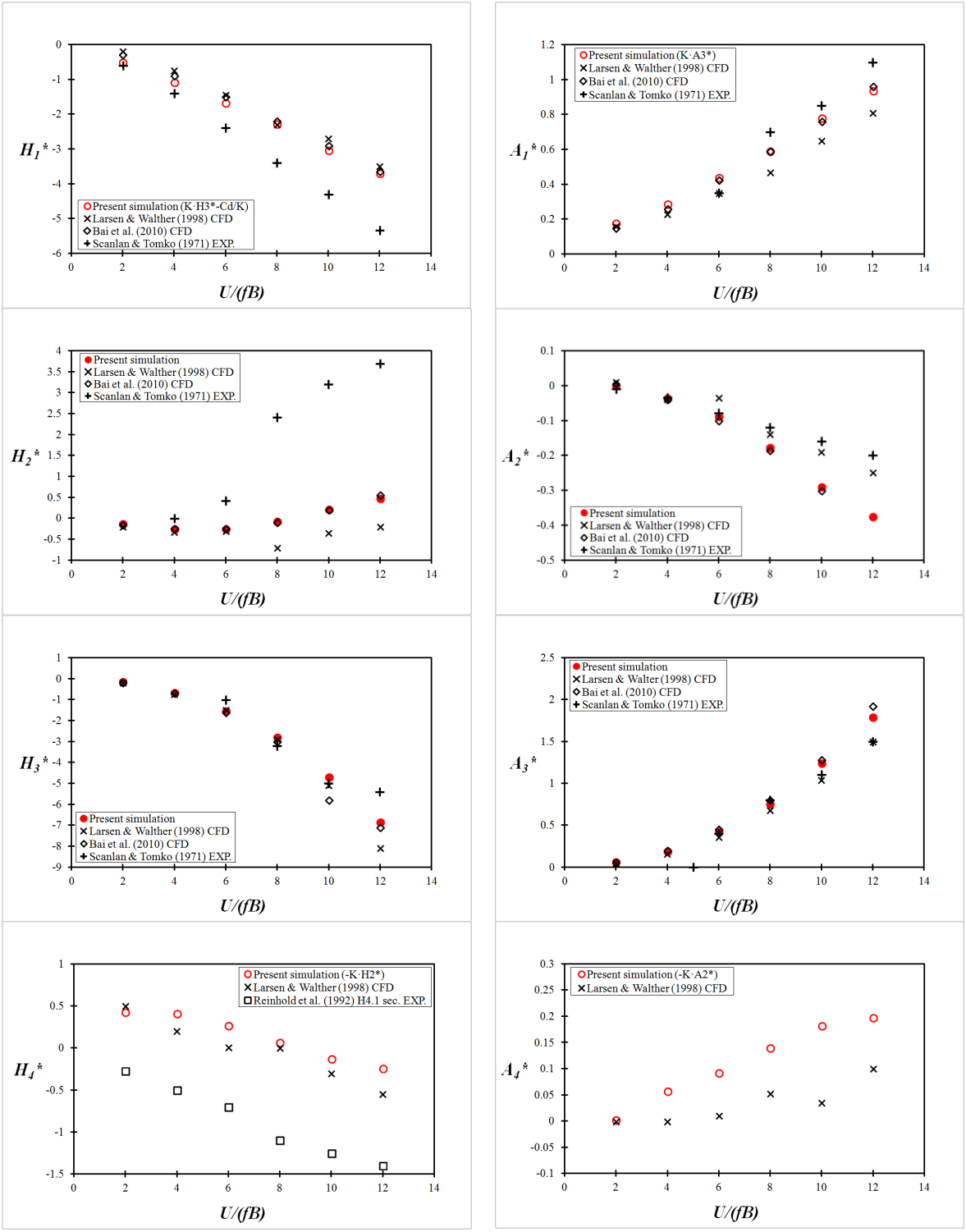

Figure 11. Flutter derivatives of the G1 generic section: numerical results and comparison with experimental (Scanlan and Tomko, 1971; Reinhold et al., 1992) and numerical (Larsen and Walther, 1998; Bai et al., 2010) data.

A very good agreement has been found for the flutter derivatives related to the pitch forced oscillation: H_3^*, A_2^* and A_3^*, which have been obtained from the numerical simulations. For the H_2^* flutter derivative, similar discrepancies as in Bai et al. (2010) have been obtained. In fact, for this flutter derivative, in the case of box decks, differences between experimental data and CFD based evaluations can be found in other references in the literature, such as Jeong and Kwon (2003), Zhu et al. (2007), Ge and Xiang (2008) or Brusiani et al. (2013). For the approximated heave-related flutter derivatives H_1^* and A_1^* the obtained results agree with wind tunnel test data and their accuracy is comparable with the other CFD-based simulations. For the flutter derivatives H_4^* and A_4^* it is more difficult to properly assess the reliability of the approximated values since experimental data are not available. It has been found that for the H_4^* flutter derivative the present simulation provides values very similar to those reported by Larsen and Walther (1998). In the same manner, the slope is almost the same as for the H4.1 experimental flutter derivative and the upwards shift of the numerical results can also be found, for instance, in Brusiani et al. (2013) where the flutter derivatives of the H4.1 section were specifically computed. For the A_4^* flutter derivative the approximated values do not show important differences in value with respect to the ones in Larsen and Walther (1998).

In order to assess the degree of accuracy in the simulations reported in this work, in table 5 the relative errors in the value of the flutter derivatives H_1^*, H_2^*, H_3^*, A_1^*, A_2^* and A_3^*, for which experimental data are available, are reported. It must be borne in mind that the data for the lower reduced velocities cannot be identified from the charts in Scanlan and Tomko (1971) for some of the flutter derivatives.

The relative errors of the numerical values taking as reference the experimental values are evaluated according to the following formula:

$$e = \frac{|exp.value - num.value|}{|exp.value|} \tag{9}$$

Table 5. Relative errors in the evaluation of the flutter derivatives of the G1 section

Flutter derivative	U_R	Present simulation	Larsen and Walther (1998)	Bai et al. (2010)
H_1^*	2	0.14	0.67	0.50
	4	0.23	0.46	0.36
	6	0.30	0.40	0.38
	8	0.33	0.32	0.35
	10	0.29	0.37	0.33
	12	0.31	0.34	0.32
H_2^*	6	1.60	1.71	1.57
	8	1.03	1.29	1.04
	10	0.93	1.11	0.94
	12	0.87	1.05	0.85
H_3^*	6	0.54	0.50	0.60

	8	0.12	0.09	0.06
	10	0.06	0.02	0.16
	12	0.27	0.50	0.31
A_1^*	6	0.25	0.00	0.21
	8	0.16	0.33	0.16
	10	0.08	0.24	0.11
	12	0.15	0.26	0.13
A_2^*	2	0.95	2.00	1.50
	4	0.03	0.14	0.14
	6	0.09	0.56	0.25
	8	0.47	0.17	0.54
	10	0.81	0.19	0.88
	12	0.88	0.25	
A_3^*	6	0.04	0.10	0.13
	8	0.06	0.15	0.00
	10	0.13	0.05	0.16
	12	0.19	0.00	0.28

From table 5, it can be concluded that the accuracy of the three simulations is equivalent, being the median of the relative errors 0.26 in the present simulation, and 0.33 and 0.32 in Larsen and Walther (1998) and Bai et al. (2010). In this respect, it is notable how the approximated values obtained using the proposed approach for the H_1^* and A_1^* flutter derivatives are comparable with the values reported in Larsen and Walther (1998) and Bai et al. (2010) where the harmonic oscillations in the heave degree of freedom were explicitly computed.

7. CONCLUDING REMARKS

In this article, the force coefficients and the flutter derivatives of an aspect ratio 4.9 rectangular cylinder and a streamlined deck type G1 cross-section have been computed based on a 2D URANS approach, applying Menter's *k-ω* SST turbulence model. A block structured mesh has been used and the open source CFD solver OpenFOAM has been applied.

The static response of the rectangular cylinder at a 0º angle of attack has agreed well with the experimental data in Schewe (2009), the RSM simulation in Ribeiro (2011) and sophisticated 2D numerical simulations where the Boussinesq assumption is substituted by an EARSM approach (Mannini et al., 2011).

For the G1 section, the influence of the spatial and temporal discretisations in the numerical results has been studied. Since both experimental and numerical results of the force coefficients and flutter derivatives are available in the literature for this particular cross-section, the current computational results have been validated against the experimental ones and also the accuracy of the simulations reported herein can be compared with CFD results published by other researchers.

The distribution of the time-averaged pressure coefficient around the G1 section agrees well with experimental data available in the literature for similar geometries. The force coefficients of the deck cross-section for angles of attack in the range -10 º and +10º have been obtained. It has been

found that they are in good agreement with the experimental and numerical data in Reinhold et al. (1992) and Bai et al. (2010).

A notable contribution of this work has been the application of the existing formulae relating the flutter derivatives (Tubino, 2005) in a CFD based approach. This has allowed the computer demands of this burdensome problem to be reduced. The pitch-related flutter derivatives have been extracted from the pitch forced oscillation simulations while the heave-related ones have been estimated using the expressions in the literature. For the two cases studied a very good agreement with the experimental flutter derivatives has been found, and at least comparable accuracy with other numerical simulations where both pitch and heave forced oscillations had been numerically computed.

This work can be considered a step forward towards the routine use of CFD based techniques in the aerodynamic and aeroelastic design of long span bridges since it has been demonstrated the adequacy of the computational results using an efficient 2D approach. Furthermore it ~~but~~ is also a step forward in the application of numerical optimization techniques in the shape design of bridges, for which efficient, reliable and computational non-cumbersome CFD techniques are a must. In this respect, a fully computational approach for the evaluation of force coefficients and flutter derivatives, as the one reported herein, is required for the application of numerical optimization techniques.

8. ACKNOWLEDGMENTS

This work has been mainly funded by the Spanish Ministry of Education, Culture and Sport under the Human Resources National Mobility Program of the R-D+i National Program 2008-2011, extended by agreement of the Cabinet Council on October 7th 2011. It has also been partially financed by the Galician Government (including FEDER funding) with reference GRC2013-056 and by the Spanish Minister of Economy and Competitiveness (MINECO) with reference DPI2013-41893-R. The authors fully acknowledge the support received.

The authors are grateful for access to the University of Nottingham High Performance Computing Facility and the Breogán Cluster at the University of La Coruña.

REFERENCES

Bai, Y., Sun, D., Lin, J. (2010) Three dimensional numerical simulations of long-span bridge aerodynamics using block-iterative coupling and DES. Computers and Fluids; 39, 1549-1561.

Bartoli, G., Mannini, C. (2008) A simplified approach to bridge deck flutter. Journal of Wind Engineering and Industrial Aerodynamics; 96, 229-256.

Brar, P.S., Raul, R., Scanlan, R.H. (1996) Numerical calculation of flutter derivatives via indicial functions. Journal of Fluids and Structures; 10, 337-351.

Braun, A.L., Awruch, A.M. (2003) Numerical simulation of the wind action on a long-span bridge deck. Journal of the Brazilian Society of Mechanical Sciences and Engineering; 25(4), 352-363.

Bruno, L., Canuto, C., Fransos, D. (2009) Stochastic aerodynamics and aeroelasticity of a flat plate via generalized Polynomial Chaos. Journal of Fluids and Structures; 25, 1158-1176.

Bruno, L., Fransos, D. (2008) Evaluation of Reynolds number effects on flutter derivatives of a flat plate by means of a computational approach. Journal of Fluids and Structures; 24, 1058-1076.

Bruno, L., Fransos, D., Coste, N., Bosco, A. (2010) 3D flow around a rectangular cylinder: a computational study. Journal of Wind Engineering and Industrial Aerodynamics; 98, 263-276.

617 Bruno, L., Khris, S. (2003) The validity of 2D numerical simulations of vortical structures around a
618 bridge deck. Mathematical and Computer Modelling; 37, 795-828.
619 Bruno, L., Khris, S., Marcillat, J. (2001) Numerical simulation of the effect of section details and
620 partial streamlining on the aerodynamics of bridge decks. Wind and Structures; 4(4), 315-332.
621 Bruno, L, Salvetti, M.V., Ricciardelli, F. (2014) Benchmark on the aerodynamics of a rectangular
622 5:1 cylinder: an overview after the first four years of activity. Journal of Wind Engineering and
623 Industrial Aerodynamics; 126, 87-106.
624 Brusiani, F., de Miranda, S., Patruno, L., Ubertini, F., Vaona, P. (2013) On the evaluation of bridge
625 deck flutter derivatives using RANS turbulence models. Journal of Wind Engineering and
626 Industrial Aerodynamics; 119, 39-47.
627 Chen, X., Kareem, A. (2002) Advances in modeling of aerodynamic forces on bridge decks.
628 Journal of Engineering Mechanics; 128, 1193-1205.
629 Davenport, A.G., King, J.P.C., Larose, G.L. (1992) Taut strip model tests. In: Larsen, A. (Ed.),
630 Proceedings of the 1st International Symposium on Aerodynamics of Large Bridges,
631 Copenhagen, Denmark.
632 Donea, J., Huerta, A., Ponthot, J.Ph., Rodríguez-Ferrán, A. (2004) Arbitray Lagrangian-Eulerian
633 methods. In Encyclopedia of Computational Mechanics. Vol 1: Fundamentals. Stein, E., de
634 Borst, R, Hughes, J.R. (Eds.). John Wiley & Sons, Ltd.
635 Frandsen, J.B. (2004) Numerical brigde deck studies using finite elements. Part I: flutter. Journal of
636 Fluids and Structures; 19, 171-191.
637 Fransos, D., Bruno, L. (2006) Determination of the aeroelastic transfer functions for streamlined
638 bodies by means of a Navier-Stokes solver. Mathematical and Computer Modelling; 43, 506-
639 529.
640 Fransos, D., Bruno, L. (2010) Edge degree-of-sharpness and free-stream turbulence scale effects on
641 the aerodynamics of a bridge deck. Journal of Wind Engineering and Industrial Aerodynamics;
642 98, 661-671.
643 Ge, Y.J., Xiang, H.F. (2008) Computational models and methods for aerodynamic flutter of long-
644 span bridges. Journal of Wind Engineering and Industrial Aerodynamics; 96, 1912-1924.
645 Holmes, J.D. (2007) Wind loading of structures. 2nd Edition. Taylor and Francis.
646 Huang, L., Liao, H., Wang, B., Li, Y. (2009) Numerical simulation for aerodynamic derivatives of
647 bridge deck. Simulation Modelling Practice and Theory; 17, 719-729.
648 Jasak, H, Rusche, H. (2009) Dynamic mesh handling in OpenFOAM. In: Fourth OpenFOAM
649 workshop. Montreal, Canada.
650 Jeong, U.Y., Kown, S. (2003) Sequential numerical procedures for predicting flutter velocity of
651 bridge sections. Journal of Wind Engineering and Industrial Aerodynamics; 91, 291-305.
652 Larose, G.L. (1992) The response of a suspension bridge deck to turbulent wind: the taut-strip
653 model approach. M. Eng. Sc., The University of Western Ontario.
654 Larsen, A., Walther, J.H. (1998) Discrete vortex simulation of flow around five generic bridge deck
655 sections. Journal of Wind Engineering and Industrial Aerodynamics; 77-78, 591-602.
656 Lesieutre, D., Reisenthel, P., Dillenius, M. (1994) A practical approach for calculating
657 aerodynamic indicial functions with Navier-Stokes solver. AIAA 94-0059.
658 Löhner, R. (2008) Applied computational fluid dynamics techniques: an introduction based on
659 finite element methods (2º Edition). John Wiley & Sons Ltd.
660 Mannini, C., Soda, A., Schewe, G. (2010) Unsteady RANS modeling of flow past a rectangular
661 cylinder: investigation of Reynolds number effects. Computers and Fluids; 30, 1609-1624.
662 Mannini, C., Soda, A., Schewe, G. (2011) Numerical investigation on the three-dimensional
663 unsteady flow past a 5:1 rectangular cylinder. Journal of Wind Engineering and Industrial
664 Aerodynamics; 99, 469-482.

665 Mannini, C., Soda, A., Voβ, R., Schewe, G. (2010) Unsteady RANS simulation of flow around a
666 bridge section. Journal of Wind Engineering and Industrial Aerodynamics; 98, 742-753.
667 Matsumoto, M. (1996) Aerodynamic damping of prisms. Journal of Wind Engineering and
668 Industrial Aerodynamics; 59, 159-175.
669 Mendes, P.A., Branco, F.A. (1998) Numerical wind studies for the Vasco da Gama Bridge,
670 Portugal. Structural Engineering International; 8(2), 124-128.
671 Menter, F., Esch, T. (2001) Elements of industrial heat transfer prediction. 16th Brazilian Congress
672 of Mechanical Engineering.
673 Morgenthal, G., McRobie, A. (2002) A comparative study of numerical methods for fluid-structure
674 interaction analysis in long-span bridge design. Wind and Structures; 5(2-4), 101-114.
675 Oliver, A. (2009) Mesh motion alternatives in OpenFOAM. PhD course in CFD with OpenSource
676 software project report. http://www.tfd.chalmers.se/~hani/kurser/OS_CFD_2009/. Accessed
677 July, 18th 2014.
678 Reinhold, T.A., Brinch, M., Damsgaard, A. (1992) Wind tunnel tests for the Great Belt Link. In:
679 Larsen, A. (Ed.), Proceedings of the 1st International Symposium on Aerodynamics of Large
680 Bridges, Copenhagen, Denmark.
681 Ribeiro, A.F.P. (2011) Unsteady RANS modeling of flow past a rectangular 5:1 cylinder:
682 investigation of edge sharpness effects. In: Proc. of the 13th International Conference on Wind
683 Engineering, Amsterdam, The Netherlands.
684 Sarkar, P.P., Caracoglia, L., Haan Jr., F.L., Sato, H., Murakoshi, J. (2009) Comparative and
685 sensitivity study of flutter derivatives of selected bridge deck sections, Part 1: analysis of inter-
686 laboratory experimental data. Engineering Structures; 31, 158-169.
687 Sarkic, A., Fisch, R., Hoffer, R. Bletzinger, K. (2012) Bridge flutter derivatives based on
688 computed, validated pressure fields. Journal of Wind Engineering and Industrial
689 Aerodynamics; 104-106, 141-151.
690 Sarkic, A., Hoffer, R. (2013) Improved numerical simulation of bridge deck aeroelasticity by
691 model validation. In: Proceedings of the Sixth European-African Conference on Wind
692 Engineering. Cambridge, UK.
693 Sarwar, M.W., Ishihara, T., Shimada, K., Yamasaki, Y., Ikeda, T. (2008) Prediction of
694 aerodynamic characteristics of a box girder bridge section using the LES turbulence model.
695 Journal of Wind Engineering and Industrial Aerodynamics; 96, 1895-1911.
696 Scanlan, R.H., Jones, N.P., Singh, L. (1997) Inter-relations among flutter derivatives. Journal of
697 Wind Engineering and Industrial Aerodynamics; 69-71, 829-837.
698 Scanlan, R.H., Tomko, J.J. (1971) Airfoil and bridge deck flutter derivatives. Journal of the
699 Engineering Mechanics Division. EM6, 1717-1737.
700 Schewe, G. (2009) Reynolds-number-effects in flow around a rectangular cylinder with aspect ratio
701 1:5. In: Borri, C., Augusti, G., Bartoli, G., Gacchini, L. (Eds.) Proceedings of the Fifth
702 European and African Conference on Wind Engineering. Firenze University Press, Florence,
703 Italy.
704 Scruton, C. (1981) An introduction to wind effects on structures. Oxford University Press.
705 Shimada, K., Ishihara, T. (2012) Predictability of unsteady two-dimensional k-ε model on the
706 aerodynamic instabilities of some rectangular prisms. Journal of Fluids and Structures; 28, 20-
707 39.
708 Simiu, E., Scanlan, R.H. (1996) Wind effects on structures. 3rd Edition; John Wiley & Sons, Inc.
709 Starossek, U., Aslan, H., Thiesemann, L. (2009) Experimental and numerical identification of
710 flutter derivatives for nine bridge deck sections. Wind and Structures; 12, 519-540.

711 Tubino, F. (2005) Relationships among aerodynamic admittance functions, flutter derivatives and
712 static coefficients for long-span bridges. Journal of Wind Engineering and Industrial
713 Aerodynamics; 93, 929-950.
714 Vairo, G. (2003) A numerical model for wind loads simulation on long-span bridges. Simulation
715 Modelling Practice and Theory; 11, 315-351.
716 Wilcox, D.C. (2006) Turbulence modeling for CFD. 3rd Edition; DCW Industries, Inc.
717 Xiang, H., Ge, Y. (2002) Refinements on aerodynamic stability analysis of super long-span
718 bridges. Journal of Wind Engineering and Industrial Aerodynamics; 90, 1493-1515.
719 Zhu, Z., Gu, M. (2014) Identification of flutter derivatives of bridge decks using CFD-based
720 discrete-time aerodynamic models. Wind and Structures; 18(3), 215-233.
721 Zhu, Z., Chen, Z., Gu, M (2009) CFD based simulations of flutter characteristics of ideal thin
722 plates with and without central slot. Wind and Structures; 12(1), 1-19.
723 Zhu, Z., Gu, M., Chen, Z. (2007) Wind tunnel and CFD study on identification of flutter
724 derivatives of a long-span self-anchored suspension bridge. Computer-Aided Civil and
725 Infrastructure Engineering; 22, 514-554.